Room-Temperature Ferromagnetism in Cu/Co Co-Doped ZnO Nanoparticles Prepared by the Co-Precipitation Method: For Spintronics Applications

Sidra Kanwal, Muhammad Tahir Khan,* Nasir Mehboob, Mongi Amami, and Abid Zaman*

Read Online

ACCESS | Metrics & More | Article Recommendations

ABSTRACT: In current work, pure ZnO and $Zn_{0.96-x}Cu_{0.04}Co_xO$ ($0 \leq x \leq 0.05$) nanoparticles were synthesized by the co-precipitation method. Structural analysis and phase determination of the formed nanoparticles was carried out using X-ray diffraction (XRD) and Williamson−Hall plots. The hexagonal wurtzite structure was manifested by all the samples with divergent microstructures. The change in lattice parameters, bond length, dislocation density, and lattice strain indicates that Cu and Co were successfully incorporated. Average crystallite size was found to be in the range of 32.16−45.42 nm for various doping concentrations. Field emission scanning electron microscopy results exhibited that the surface morphology is an amalgam of spherical-like and hexagon-like structures. Spherical-shaped grains were homogeneous and evenly distributed all over the structure. Fourier transform infrared spectra indicated that the absorption bands were blue-shifted with increasing Co concentration. The UV−visible absorption spectra showed high absorption in the UV region and weak absorption in the visible region. An increase in the energy band gap for the maximum absorption peak was observed from 3.49 eV for ZnO to 3.88 eV for $Zn_{0.91}Cu_{0.04}Co_{0.05}O$. The Burstein−Moss effect explained the noticed blue shift in absorption spectra and energy band gaps. The vibrating sample magnetometer study revealed the change in the diamagnetic behavior of pure ZnO to the ferromagnetic behavior of the prepared nanoparticles at room temperature for different doping concentrations. In the current study, we have developed the room-temperature ferromagnetism (RTFM) for Cu and Co co-doped ZnO nanoparticles. Since RTFM is the key objective for dilute magnetic semiconductors, therefore it can be served as the desirable expectant for spintronics applications with improved functionalities and device concepts.
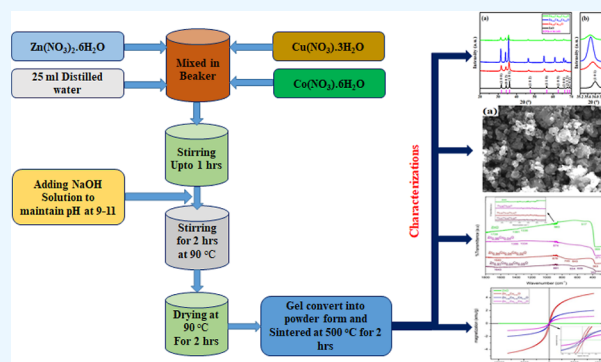
INTRODUCTION

In recent years, spin-based electronics has become a topic of interest for technological applications due to the increasing degree of freedom in these specialized tools. It is an emerging domain that is providing a combination of spin and charge of electrons, which was previously unavailable.[1] The science of spintronic devices is based on enhanced electronic, magnetic, and optical properties of semiconductors in order to reduce their power consumption and to increase their memory and processing capabilities in comparison to traditional electronics. These properties can be tuned by doping suitable magnetic materials into host semiconductors. The developed magnetic semiconductors can be used as electronic devices, which possess both spin and charge characteristics.[2] Due to this special character, these materials can be used in logic function gates and storage devices. Diluted magnetic semiconductors (DMSs) represent an association between charge-based semiconductors and spin-based magnetism.[3,4] Many theoretical and experimental investigations have supported the fact

that when a wide-band gap semiconductor (ZnO) is doped with transition metals (TMs) like Cu, Fe, Co, Ni, Mn, Cr, and V, dilute magnetic semiconductors are formed.[5] DMSs could combine storage, detection, logic, and communication capabilities to fabricate a multifaceted device that can substitute various components designed for these purposes. Also, the optical properties of DMSs for transforming magnetic data into an optical signal has been a specific point of interest.[6]

ZnO is a transparent metal oxide with several peculiar properties like a large exciton binding energy of 60 meV and a direct band gap of ~3.4 eV. There are numerous uses of ZnO in transparent conducting oxide (TCO), solar panels, ultra-

violet lasers, light modulators, transducers, piezoelectric devices, light emitting diodes (LEDs), and others.[7] As ZnO is biocompatible and biodegradable, so it is also suitable for medical purposes. The metal oxide semiconductors doped with TM can fulfill the properties of required dilute magnetic semiconductors having a combination of ferromagnetic long-range order and semiconducting behavior in a single phase. Doping is a pivotal factor for the enhancement of structural, morphological, magnetic, electrical, and optical features of ZnO.[8,9] This can be achieved by adding impurities either noble metals (e.g., Pd, Ag, Pt, etc.) or TMs (e.g., Al, Cr, Mn, Fe, Ni, Cu, Co, etc.). Room-temperature ferromagnetism (RTFM) is a demanding phenomenon now a days, which can be pulled off by the addition of impurities in TM (TMs are d-block elements occupying the center of the periodic table between group 2A and 3A, having partially filled d-orbitals and variable oxidation states). Among all the TMs, we have doped Co and Cu in pure ZnO because of the property of appreciable variation in band gaps by minor change in doping percentage, which influences the optical and magnetic properties of NPs. An enhanced ferromagnetic order has also been observed for this combination in the literature. Jayakumar et al. showed that the co-doping of Cu with Co increases the carrier concentration considerably, and the ferromagnetism was enhanced by additional carriers.[10] Enhanced ferromagnetic order was observed for Cu and Co co-doped ZnO powders, and it was related to the high density of oxygen vacancy defects.[11] The origin of ferromagnetism in (Co, Cu): ZnO has been attributed to a defect-related mechanism,[12] whereas theoretical calculation results showed that the antiferromagnetic state is higher in energy than the ferromagnetic state in the ZnO/Cu system.[10,13] However, according to first-principles calculations, the suitable amount of Cu doping suggests a ferromagnetic ground state.[14,15]

Pure ZnO nanorods are diamagnetic in nature, which is also confirmed in our experiment. Although some research work is already available in the literature on the Cu and Co co-doped ZnO system, but nearly, all the work on thin films and extensive examination of structural, optical, and magnetic features is insufficient.[16] Also, the abovementioned discrepancies regarding the origin of RTFM in Cu/Co co-doped ZnO nanoparticles are still to be addressed.

Numerous synthesis methods have been dedicated to the modeling of TM-doped ZnO nanoparticles, such as the sol−gel method, co-precipitation method, an auto-combustion method, hydrothermal process, solid−state reaction method, low-temperature solution process, rapid synthesis, and many others.[17−19] Among all of them, we have employed the co-precipitation method because it attracts more attention due to its unique advantages including low cost, simple laboratory equipment, easy adjustment of dopant concentration, and large-scale synthesis of nanoparticles. Also, in this technique, different parameters like reaction time, reaction temperature, and pH−concentration of the material have remarkable influence on the NP's shape and size characteristics.

Hence, in this research, our objective is to study the repercussions of Co co-doping along with Cu in ZnO on structural and magnetic properties without disturbing the host's crystalline structure and development of RTFM for practical applications.

RESULTS AND DISCUSSION

X-ray Diffraction. Figure 1a displays the XRD spectra of ZnO, $Zn_{0.96}Cu_{0.04}O$, $Zn_{0.94}Cu_{0.04}Co_{0.02}O$, and
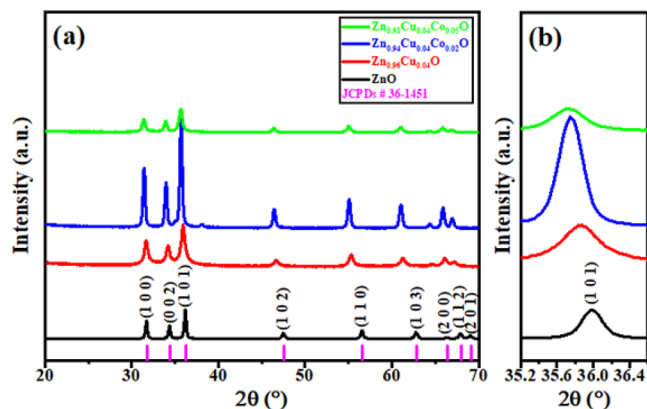
Figure 1. (a) XRD patterns of ZnO, $Zn_{0.96}Cu_{0.04}O$, $Zn_{0.94}Cu_{0.04}Co_{0.02}O$, and $Zn_{0.91}Cu_{0.04}Co_{0.05}O$ nanoparticles and (b) zoomed view of (1 0 1) peak shifting toward the lower angle.

$Zn_{0.91}Cu_{0.04}Co_{0.05}O$ nanoparticles. The hexagonal wurtzite structure is confirmed from the typical diffraction peaks for (1 0 0), (0 0 2), and (1 0 1) planes located at 32.5, 35.5, and 37.3° of 2θ, respectively, with a high degree of crystallization and approximately similar to the standard data of pure ZnO (a = 3.2488 Å, c = 5.2061 Å, space group $P63mc$) and very well-matched with JCPDS # 36-1451.[20] The XRD spectrum shows three broad peaks indexed as (1 0 0), (0 0 2), and (1 0 1) for each sample, showing that the nature of the prepared nanoparticles is polycrystalline. In all the samples, nine major peaks are observed, which are indexed as (1 0 0), (0 0 2), (1 0 1), (1 0 2), (1 1 0), (1 0 3), (2 0 0), (1 1 2), and (2 0 1) with maximum diffraction intensity at (1 0 1) lying between 35.8 and 37.6°. A left shift in the highest peak of the (101) plane is observed for all samples (Figure 1b) with the increase in the concentration of co-dopant concentration of Co and Cu in pure ZnO. This shift could have occurred due to structural changes occurring in the crystal structure of ZnO due to doping.[21] The calculated crystallographic parameters are given in Table 1.

In this study, the XRD peaks are shifted to the lower angle with increasing co-dopant concentration of Co and Cu in pure ZnO. The reason for this is the variation of the ionic radii of Zn^{2+} (0.60 Å), Co^{2+} (0.58 Å), and Cu^{2+} (0.73 Å). We have determined the average crystal size by using Debye Scherer's equation[22]

$$average\ crystal\ size\ (D) = \frac{0.9\lambda}{\beta\ \cos\theta} \quad (1)$$

where, λ is the wavelength of the incident radiation, that is, 1.45 Å, β is the full width at half maximum (FWHM) of the (101) peak, and θ is Bragg's angle.

ZnO bond length is calculated by using the following equation

$$L = \sqrt{\left(\frac{a^2}{3}\right) + (0.5 - u)^2 c^2} \quad (2)$$

Table 1. Lattice Parameters $a = b$ (Å), c (Å), c/a Ratio, 2θ, FWHM Values, d-Spacing, Crystallite Size, Bond Length, and Volume of ZnO, $Zn_{0.96}Cu_{0.04}O$, $Zn_{0.94}Cu_{0.04}Co_{0.02}O$, and $Zn_{0.91}Cu_{0.04}Co_{0.05}O$ Nanoparticles from the XRD Profile

sample	2θ (degrees)	$a = b$ (Å)	c (Å)	c/a	FWHM (°)	d-spacing (Å)	bond length (Å)	volume (Å)³
ZnO	37.07	3.2472	5.2133	1.6052	0.3577	2.493	2.160	47.60
$Zn_{0.96}Cu_{0.04}O$	36.36	3.249	5.20661	1.6021	0.4535	2.4629	1.977	47.59
$Zn_{0.94}Cu_{0.04}Co_{0.02}O$	36.27	3.2498	5.20661	1.6022	0.3211	2.4629	1.978	47.596
$Zn_{0.91}Cu_{0.04}Co_{0.05}O$	36.45	3.2498	5.20661	1.6022	0.48242	2.4629	1.976	47.595

where "a" and "c" are lattice constants and "u" is the constant for the wurtzite structure that can be calculated using the following relation

$$u = \left(\frac{a^2}{3c^2}\right) + 0.25 \tag{3}$$

Also, the unit cell volume is computed by using the following equation

$$V = 0.866a^2c \tag{4}$$

Average crystallite size initially decreases by doping Cu in pure ZnO (from 38.43 to 32.16 nm), which is due to the disfigurement of the ZnO lattice with doped impurity, which results in decreasing the nucleation of ZnO nanoparticles.[23] Then, there is an increase in the crystal size when Co is doped in the Zn−Cu−O crystal because the ionic radius of Co^{2+} (0.58 Å) is comparable to the ionic radii of Zn^{2+} (0.60 Å) and Cu^{2+} (0.73 Å).[24] Initially, the increase in intensity of the peak showed that the intrinsically agglomerating Co^{2+} ions lead to the growth of the ZnO particles and alter the crystallization of the ZnO. The lattice distortion around Co atoms in Zn−Cu−O is responsible for a very low-intensity peak below 2% concentration of Co and reduction in crystal size. The enhancement in the peak intensity and the decrease in FWHM beyond Co 2% are directly pointing to the enhancement of the crystallinity of the nanoparticles. Further doping of Co comforted the tensile stress, and the lattices were comparatively relaxed, giving rise to the quality of crystallization, and the crystal size also decreased.[17] With the doping of cobalt 5%, the peak position enhanced but the peak intensity reduced as compared to those of cobalt 2%; it is because of the microstrain and increased crystal size.[25] Upon incorporation of Co, the peak slightly shifted toward the lower angle, indicating the minute variability in the ionic radii of Co and Zn and that the Co^{2+} substitutes the Zn^{2+} ions without altering the wurtzite structure.[26]

In Figure 2, the alteration of FWHM and average crystal size for all the samples is shown. The FWHM value shows the inverse trend as it increased from 0.3577 to 0.4535°, and the average particle size was reduced from 38.43 to 32.16 nm with the addition of Cu in the ZnO crystal lattice. It is the indication of the presence of nano-sized particles in the samples. The reduction in the particle size is mainly due to the distortion of the host ZnO lattice with the foreign impurity, that is, Cu^{2+} which decreases the nucleation and subsequent growth rate with the addition of Cu concentrations.[24] The observed larger particle size (45.42 nm) and the smaller FWHM value (0.3211°) for Co = 2% are attributed to the combined effect of Co^{2+} incorporation at the Zn^{2+} site along with the formation of the CuO phase. The FWHM increases again on increasing the cobalt concentration to 5%, showing deformity in the lattice and limiting the additional solubility of Co in Zn−Cu−O.[25]
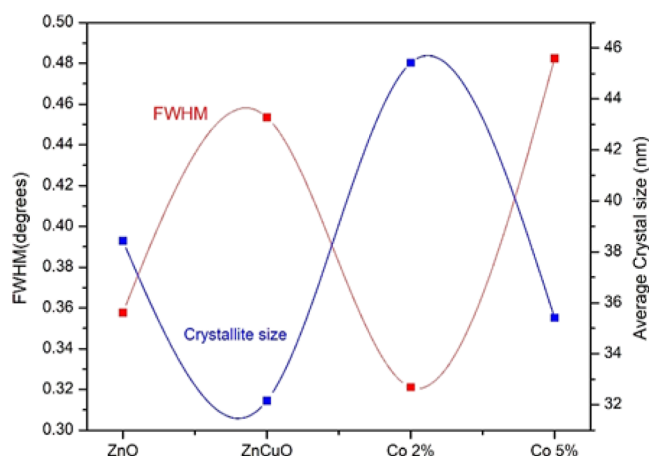
Figure 2. FWHM and average crystallite size of ZnO, $Zn_{0.96}Cu_{0.04}O$, $Zn_{0.94}Cu_{0.04}Co_{0.02}O$, and $Zn_{0.91}Cu_{0.04}Co_{0.05}O$ nanoparticles.

Sharp peaks in the spectrum are the indication of a high degree of crystallization in all the samples. The missing secondary phase linked to magnetic precipitate revealed the intrinsic ferromagnetic behavior.[16] For Co above 2%, the possession of the secondary phase in the X-ray diffraction pattern depicts the solubility limit of Co in the Cu-doped ZnO lattice. No variation in the hexagonal wurtzite structure with Co doping has been noticed as the c/a ratio is persistent for all the samples.[26,27] Table 1 shows different parameters obtained from XRD data.

The deviation in the calculated lattice strain and crystallite sizes of all the prepared pure ZnO and Cu/Co co-doped ZnO nanoparticle samples with compositions is given in Table 2. The estimated average crystallite sizes were found to be in the 32.16−45.42 nm range.

Table 2. Calculated Average Crystallite Size (D), Microstrain (ε), Dislocation Density(δ), and Lattice Strain (η) of ZnO, $Zn_{0.96}Cu_{0.04}O$, $Zn_{0.94}Cu_{0.04}Co_{0.02}O$, and $Zn_{0.91}Cu_{0.04}Co_{0.05}O$

composition	D (nm)	ε ($\times 10^{-3}$)	δ ($\times 10^{-3}$ nm⁻²)	η ($\times 10^{-3}$)
ZnO	38.43	1.307	6.7711	0.8221
$Zn_{0.96}Cu_{0.04}O$	32.16	3.375	9.6687	2.0524
$Zn_{0.94}Cu_{0.04}Co_{0.02}O$	45.42	1.455	4.8474	1.0488
$Zn_{0.91}Cu_{0.04}Co_{0.05}O$	35.41	2.113	7.9753	1.2986

Mathematically, the dislocation density (δ) and microstrain (ε) of the highest peak in all samples was calculated by using these equations[28]

$$\delta = \frac{1}{D^2} \tag{5}$$

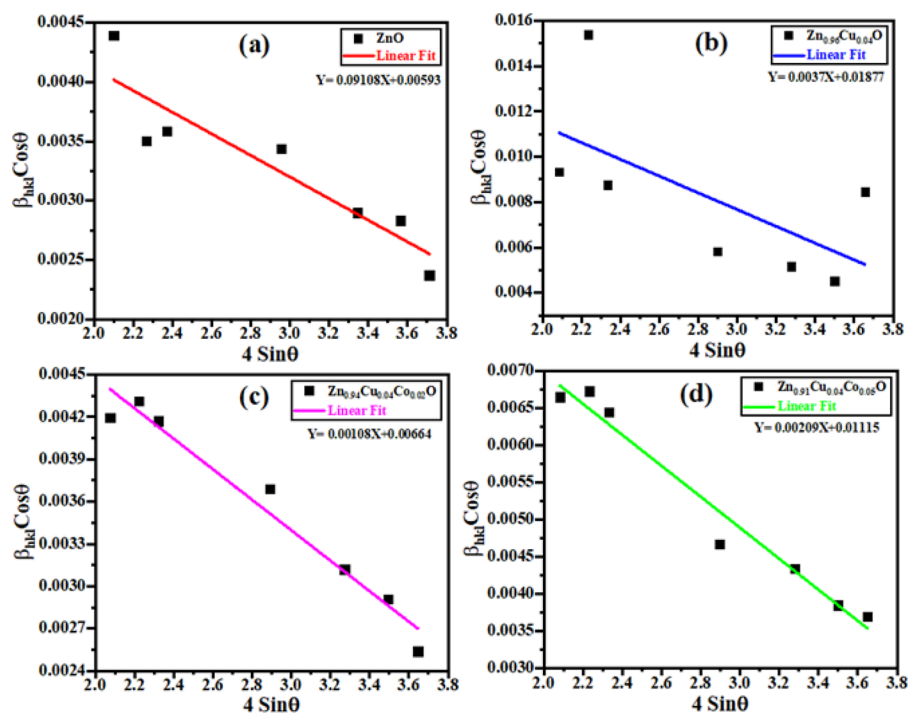$$\varepsilon = \frac{\beta}{4 \tan \theta} \tag{6}$$

Figure 3. Williamson–Hall (W–H) plots of (a) ZnO, (b) $Zn_{0.96}Cu_{0.04}O$, (c) $Zn_{0.94}Cu_{0.04}Co_{0.02}O$, and (d) $Zn_{0.91}Cu_{0.04}Co_{0.05}O$.
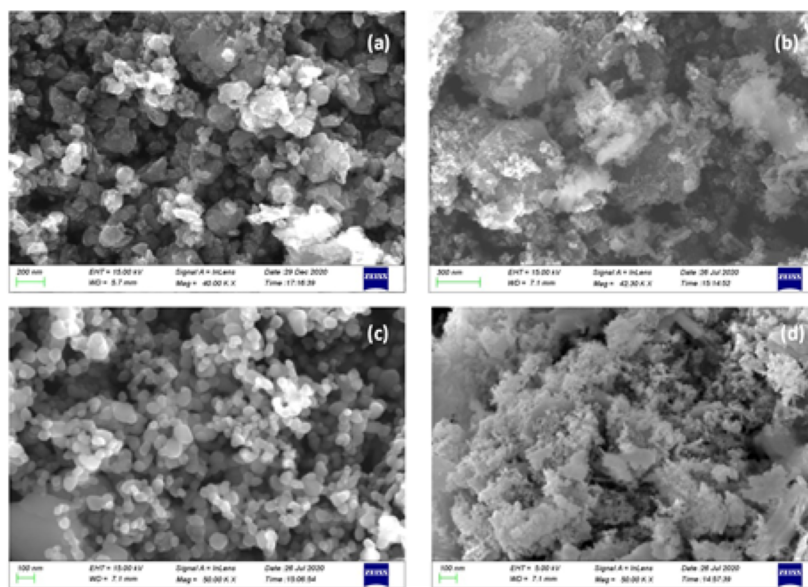
Figure 4. SEM micrographs of (a) ZnO, (b) $Zn_{0.96}Cu_{0.04}O$, (c) $Zn_{0.94}Cu_{0.04}Co_{0.02}O$, and (d) $Zn_{0.91}Cu_{0.04}Co_{0.05}O$ nanoparticles.

The lattice strain (η) was calculated through the given equation[29]

$$\eta = \frac{\beta \cos \theta}{4} \tag{7}$$

It was found from the calculated values $\delta = \frac{1}{D^2}$ that the dislocation density increases with the increase in dopant concentration. The smallest dislocation density 0.0048474 nm^{-2} was exhibited by $Zn_{0.94}Cu_{0.04}Co_{0.02}O$, while the highest dislocation density 0.0096687 nm^{-2} was exhibited by $Zn_{0.96}Cu_{0.04}O$. The increase in the "δ" value is caused by the atoms of dopants settled inside the host ZnO matrix. Furthermore, the increase in the dopant concentration causes

movement of atoms from grain boundaries to crystallites.[30] Therefore, the increase in "δ" with increasing dopant concentration may also be due to the movement of Cu and Co atoms from grain boundaries to crystallites.

The particle size and lattice strain of pure ZnO and Cu/Co co-doped ZnO nanoparticle samples were determined using the Williamson–Hall technique from the broadening of the XRD peaks.[31]

$$\beta \cos \theta = \frac{k\lambda}{D} + 4\varepsilon \sin \theta \tag{8}$$

where β is the FWHM in radian by fitting the prominent peaks, θ is the diffraction angle in radian, k is the shape factor value
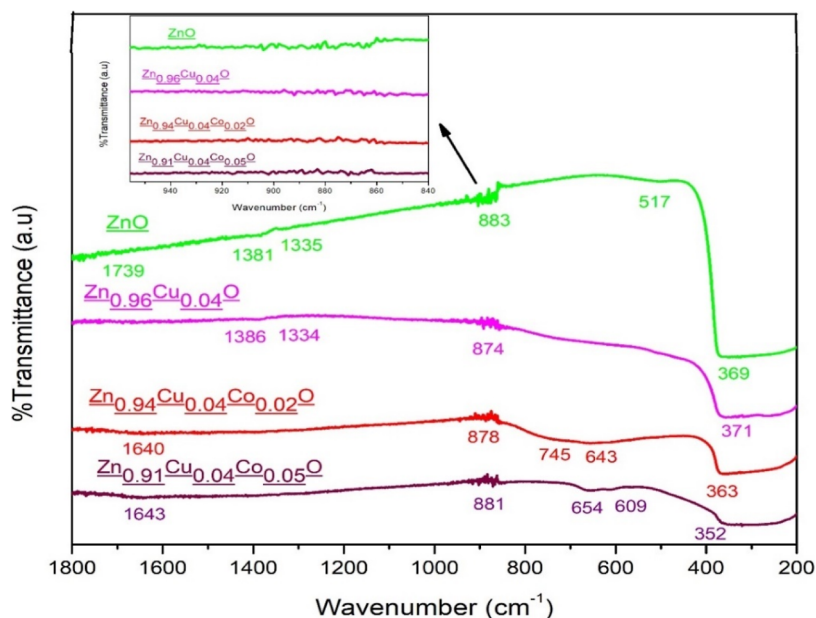
Figure 5. FTIR spectra from 1800 to 200 cm^{-1} of ZnO, Zn$_{0.96}$Cu$_{0.04}$O, Zn$_{0.94}$Cu$_{0.04}$Co$_{0.02}$O, and Zn$_{0.91}$Cu$_{0.04}$Co$_{0.05}$O nanoparticles. The inset shows the zoomed view of transmission peaks in the range (955−840) cm^{-1}.

Table 3. IR Transmission Peaks and Their Assignments of ZnO, Zn$_{0.96}$Cu$_{0.04}$O, Zn$_{0.94}$Cu$_{0.04}$Co$_{0.02}$O, and Zn$_{0.91}$Cu$_{0.04}$Co$_{0.05}$O Nanoparticles

|	wavenumber (cm^{-1})			
assignments	ZnO	Zn$_{0.96}$Cu$_{0.04}$O	Zn$_{0.94}$Cu$_{0.04}$Co$_{0.02}$O	Zn$_{0.91}$Cu$_{0.04}$Co$_{0.05}$O
Zn−O bond (tetrahedral)	369	371	363	352
Zn−O bond (octahedral)	517	550	Absent	609
Co−O stretching mode and ethanol precursors	640	734	643,745	654
microstructural changes	883	874	878	881
H−O−H bending vibration	1739	1714	1640	1643

0.94, "λ" is the XRD wavelength (λ = 0.15418 nm), and "D" is the effective crystalline size. Figure 3a−d shows the pure ZnO and Cu/Co co-doped ZnO nanoparticle samples; the slope of linear data plotted fits against 4sin θ versus β cos θ and contributes the information about the inverse of the intercept, and lattice strain yields the value of crystalline size (D_{W-H}).[32] The W−H is used for deconvoluting shapes (crystalline shapes) and strain that contributes to X-ray line broadening because Scherrer's formula does not take into account the strain contribution. The points are noted to be narrow-spaced around the fitted line. It has been observed that certain additional parameters of the analyzed sample were not taken into the consideration, or alternative techniques should be used.

Surface Morphology. Scanning electron microscopy images of ZnO, Zn$_{0.96}$Cu$_{0.04}$O, Zn$_{0.94}$Cu$_{0.04}$Co$_{0.02}$O, and Zn$_{0.91}$Cu$_{0.04}$Co$_{0.05}$O nanoparticles are shown in Figure 4. The surface morphology of sample ZnO in Figure 4a is a blend of spherical-like and hexagonal-like structures. However, with Cu substitution, spherical-shaped grains can be seen in Figure 4b, which are homogeneous. Figure 4c exhibits small petal-like structures distributed throughout the surface. Figure 4d reveals the spherical distribution being randomly dispersed all over the surface, whereas it forms a densely packed network. The grain size of the undoped sample is about 32 nm, and the grain size of the doped samples is around ~20 nm, and these results correlate with our XRD results. The grain size reduced with the increase in cobalt doping concentration.[33] Vijayaprasath et al. also reported the decrease in average grain size with increasing doping concentration in Co-doped Ni/ZnO nanoparticles.[34] Here, it was noticed that the dopant decreased the degree of crystallization through its substitution. The samples with higher doping possess poor crystallinity; it is may be due to the lower ionic radii of Co as compared to that of Zn.[35]

Fourier Transform Infrared Study. FTIR is an approach to attain particulars about the chemical bonding of material and to investigate the elemental constituents. The band locations and number of absorption peaks primarily depend upon chemical configurations and morphological configurations.[36] Figure 5 shows the FTIR spectra from 200 to 1800 cm^{-1} of ZnO, Zn$_{0.96}$Cu$_{0.04}$O, Zn$_{0.94}$Cu$_{0.04}$Co$_{0.02}$O, and Zn$_{0.91}$Cu$_{0.04}$Co$_{0.05}$O nanoparticles. Table 3 shows different modes and assignments of infrared peaks obtained for all the samples. The absorption peaks above 1000 cm^{-1} are ascribed to usual polymeric O−H stretching vibration of H$_2$O in the Cu−Co−Zn−O lattice, and the chemical bonding corresponds to the tetrahedral mode, which is designated to a little amount of water in ZnO nanocrystals and moisture present in the atmosphere.[37]

By adding Co into the Zn−Cu−O lattice, the modification in microstructural features produces vibrational frequencies, creating medium to weak bands around 600−900 cm^{-1}. Also, the bond structure changes to the octahedral mode in this region.[38] At the frequency around 600−900 cm^{-1}, the variation
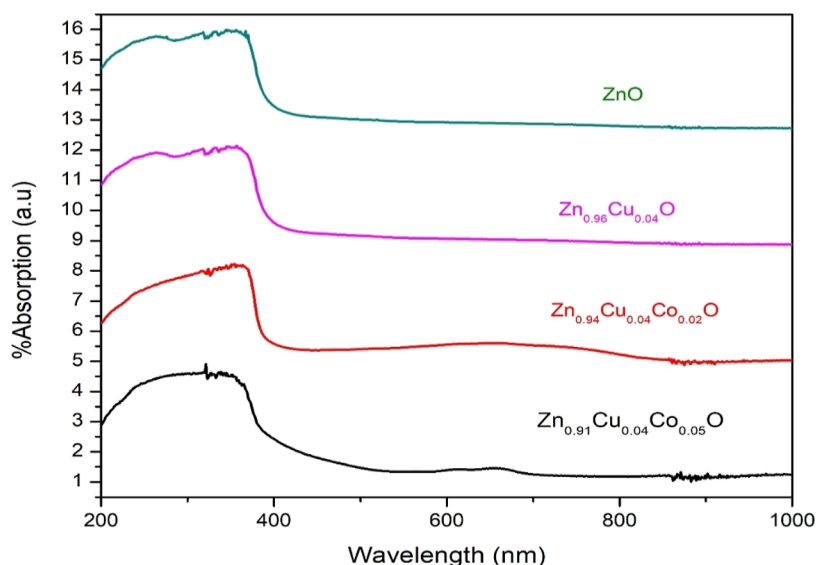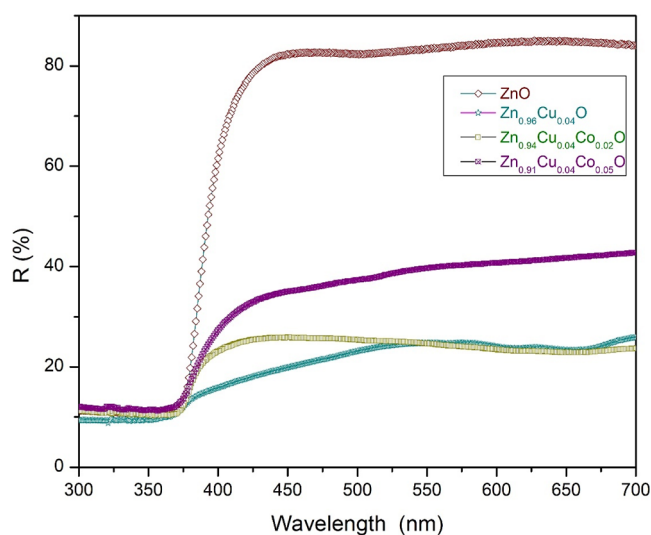
Figure 6. UV−visible absorption spectra of ZnO, $Zn_{0.96}Cu_{0.04}O$, $Zn_{0.94}Cu_{0.04}Co_{0.02}O$, and $Zn_{0.91}Cu_{0.04}Co_{0.05}O$ nanoparticles as a function of wavelength from 200 to 1000 nm.

in FWHM and intensity reveals a deviation in defect state density in the Zn−Cu−Co−O lattice. With increasing Co concentration, the transmittance % increased and was highest for Co = 5%. The strong vibrations are due to stretching frequency of Co−O and microstructural changes from 800 to 900 cm^{-1}. Co atoms are a bit lighter than Zn atoms; that is why more substitution leads to an upward shift in stretching frequency. The deviation in the transmittance % of Co−O and Zn−O bands and the characteristic frequency speculates that the addition of Co perturbs the structure of the Zn−O−Cu lattice.[39] Therefore, it is evident from the FTIR results that Co successfully occupies the Zn position in ZnO matrix as seen in XRD results and the Zn−Cu−O bond is perturbed due to the involvement of Co in its environment.

Optical Study. The reflectance spectra of ZnO, $Zn_{0.96}Cu_{0.04}O$, $Zn_{0.94}Cu_{0.04}Co_{0.02}O$, and $Zn_{0.91}Cu_{0.04}Co_{0.05}O$ nanoparticles obtained by UV−vis diffuse reflectance spectroscopy (DRS) in the range of 300−700 nm wavelength are shown in Figure 7. Notice that all the graphs in Figure 7 have an absorption edge close to 360 nm, which is similar for the band gap of ZnO.[40] Maximum reflectance (∼80%) was observed for ZnO nanoparticles, and it considerably reduced on doping Cu and then slightly increased with increasing Co concentration. At room temperature, optical absorption spectra have also been taken in the wavelength range 200−1000 nm as exhibited in Figure 6. The absorbance strongly depends on numerous aspects, like band gaps, impurities, oxygen deficiency, and roughness of the surface.

Strong UV absorption peaks at wavelengths 356, 353, 348, and 319 nm are remarked for ZnO and $Zn_{0.96-x}Cu_{0.04}Co_xO$ with Co 0%, 2%, and 5%, respectively, and can be generated from the recombination of localized-level excited electrons below the conduction band with the holes in the valence band. Increased Co doping lowers the potency of UV absorption, and the highest intensity is noticed at Co = 2%-doped $Zn_{0.96}Cu_{0.04}O$ nanoparticles. The increase in distortion cautiously decreased the absorption, which also affected the carrier density. Table 4 shows the values of energy band gaps corresponding to the wavelength of prominent absorption peaks obtained for all the samples. Expansion in energy band

Figure 7. Reflectance spectra of ZnO, $Zn_{0.96}Cu_{0.04}O$, $Zn_{0.94}Cu_{0.04}Co_{0.02}O$, and $Zn_{0.91}Cu_{0.04}Co_{0.05}O$ nanoparticles as a function of wavelength from 300 to 700 nm.

Table 4. Values of Energy Band Gaps Corresponding to the Wavelength of the Absorption Peak for all the Samples

samples	absorption peak λ (nm)	energy band gap E_g (eV)
ZnO	356	3.49
$Zn_{0.96}Cu_{0.04}O$	353	3.51
$Zn_{0.94}Cu_{0.04}Co_{0.02}O$	348	3.56
$Zn_{0.91}Cu_{0.04}Co_{0.05}O$	319	3.88

gaps from 3.49 to 3.88 eV has been observed with the doping of Cu in ZnO and increasing Co concentration in Zn−Cu−O nanoparticles. Also, with the substitution of Co^{2+} ions, a minor shift in UV peaks is noticed toward the lower wavelength, which can be allocated to the blue shift of energy gaps with Co doping. The Burstein−Moss effect can explain the blue shift in the UV absorption peak, which states that, by increasing carrier concentration in degenerately doped semiconductors, the

Fermi level merges into the conduction band, and as a result, the apparent band gap increases and the absorption edge is propelled toward higher energies.[41]

It also has been acknowledged that, on the nanometer scale, the physical properties of the semiconductor materials undergo changes, known as the "quantum confinement effect" of nanoparticles, and this confinement increases the band gap energy.[42] As the absorption edge is pushed to higher energies, the apparent band gap rises as an outcome of some states close to the conduction band being occupied.[43] The Fermi level combines to the conduction band with greater carrier concentration, increasing the band gap with further doping. Since the degree of band gap change is dependent on the crystallite size, so the "quantum confinement effect" has more contribution to the widened band gap of ZnO. The results are in accordance with the results available in the literature.[44]

Vibrating Sample Magnetometer (Magnetic Properties). Magnetic properties were examined using a vibrating sample magnetometer (VSM) at room temperature. Magnetic properties of dilute magnetic substances depend mainly upon the synthesis technique, doping element, and annealing temperature. Figure 8 displays the correspondence between
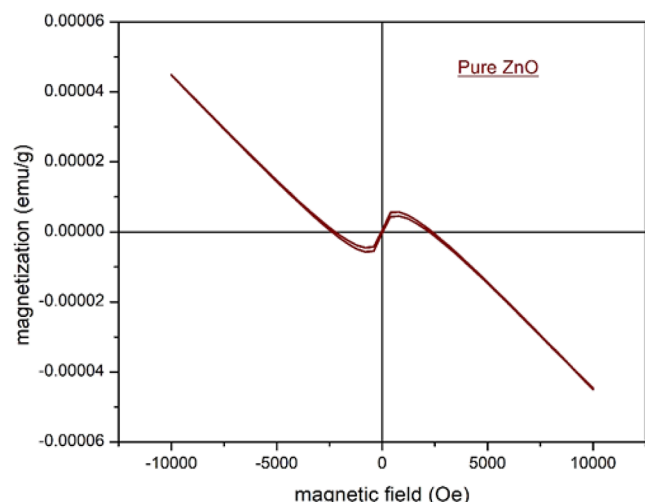

Figure 8. Vibrating sample magnetometer results of pure ZnO.

Figure 9. VSM results of ZnO, $Zn_{0.96}Cu_{0.04}O$, $Zn_{0.94}Cu_{0.04}Co_{0.02}O$, and $Zn_{0.91}Cu_{0.04}Co_{0.05}O$ nanoparticles. The inset shows the zoomed view of M-H loops of the samples.

magnetic flux density B and magnetizing force F commonly called M-H loops. Magnetic investigations proved that all ZnO and CuO composites have room-temperature ferromagnetism and undoped ZnO is diamagnetic at room temperature, as depicted in Figure 8. Potzger et al. revealed that all of the undoped ZnO samples are absolutely diamagnetic in nature over magnetization reversal, even at low temperature (5 K).[45] The transformation of diamagnetism of the pure ZnO sample into ferromagnetic nature of the Cu and Co co-doped ZnO sample pinpoints the desired favorable substitution of Co atoms in the ZnCuO lattice (Figure 9).

No clustering and surface agglomerations or any other secondary phases are observed around Zn−Cu−O particles, indicating the intrinsic ferromagnetic behavior of the Cu, giving rise to RTFM. The bond length and volume are decreased by the doping of Co into the Zn−Cu−O lattice (as shown in Table 1), resulting in a decrease in the comparative distance between Cu ions and strengthening the antiferromagnetic order. This intensified antiferromagnetic interaction between neighboring Cu−Cu ions is the main cause of the
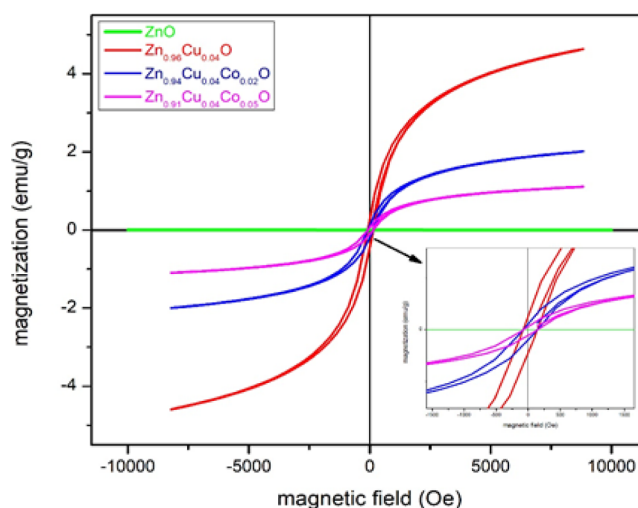
suppression of RTFM at high doping concentration.[46] The observed RTFM is the result of homogeneous doping of Co in Zn−Cu−O particles, which is in accordance with the Ruderman−Kittel−Kasuya−Yosida (RKKY) mechanism referring to a coupling mechanism of nuclear magnetic moments or localized inner d- or f-shell electron spins in a metal by the interaction through conducting electrons.

A clear ferromagnetism is achieved at room temperature for doped samples. All the doped samples formed an S loop, which is the evidence of RTFM but the doping of Co decreases the saturation magnetization and retentivity of the samples as shown in Table 5.[47] However, Wei et al. reported the opposite

Table 5. Values of Saturation Magnetization and Retentivity of the Doped Samples

sample	M_s (emu/g)	M_r (emu/g)
$Zn_{0.96}Cu_{0.04}O$	4.632	0.255
$Zn_{0.94}Cu_{0.04}Co_{0.02}O$	2.014	0.108
$Zn_{0.91}Cu_{0.04}Co_{0.05}O$	1.108	0.057

trend for different Cu concentrations in Co and Cu co-doped ZnO powders. They observed an increase in the values of saturation magnetization and retentivity with increasing Cu concentration.[48] Figure 10 shows the influence of Co doping concentration on the magnetization of the nanoparticles. Also, the hysteresis loop became narrow with increasing doping percentage. The narrow hysteresis is an indication of small amount of energy dissipation in reversing the magnetization, which is the key for rapid magnetization and demagnetization of the synthesized samples. There can be various reasons for RTFM in Cu and Co co-doped ZnO nanoparticles. Cao et al. illustrated that p-type carriers introduced by Cu doping are considered to be a main factor inducing RTFM.[49] Spaldin suggested that robust ferromagnetism will only be obtained in TM-doped ZnO if p-type carriers are also included. The hole-induced ferromagnetism in ZnCoO has already been observed with Li doping.[50,51] The point defects such as Zn interstitials and oxygen vacancies can also be the possible reasons for RTFM.[52] However, in our case, there are no clustering and other phases observed in the XRD spectrum and no evidence
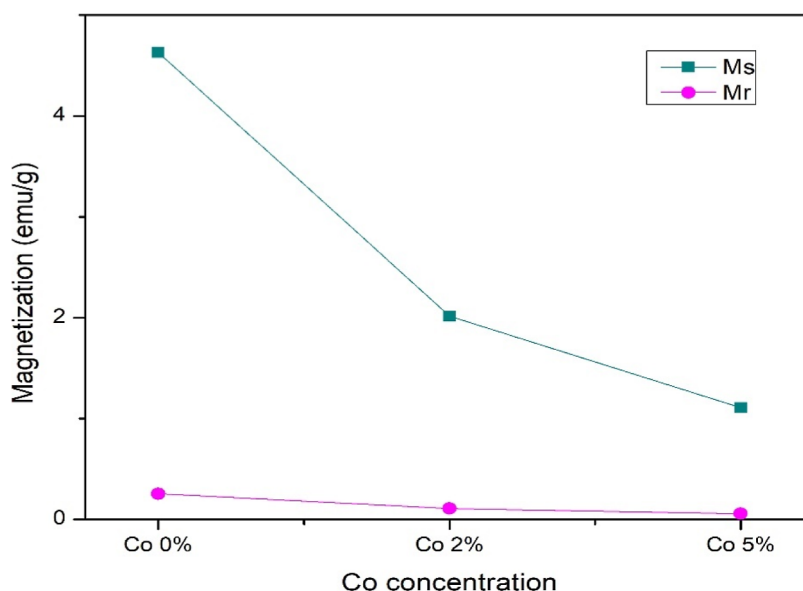
Figure 10. Influence of Co doping on the magnetization of Cu/Co co-doped ZnO nanoparticles.

of oxygen vacancies is detected; hence, the ferromagnetic ordering in our samples is not the consequence of secondary phases or clustering. Therefore, this study also revealed the fact that the room-temperature ferromagnetic conduct noticed in the Cu and Co co-doped ZnO nanoparticles is an intrinsic property. Similar results have been observed for Cu/V co-doped ZnO nanoparticles by Liu et al.[53]

CONCLUSIONS

The co-precipitation method was employed to synthesize pure ZnO and Cu/Co co-doped ZnO nanoparticles $Zn_{0.96-x}Cu_{0.04}Co_xO$, x = 0, 0.02, and 0.05. All the samples manifested the hexagonal wurtzite structure with divergent microstructures. Crystallite size initially decreases from 38.43 to 32.16 nm and then increases to 45.42 nm and again decreases to 35.41 nm, which confirms the deformity in the lattice and limits the additional solubility of Co in Zn−Cu−O. Values of dislocation density and microstrain are higher for doped samples as compared to those of the undoped samples, indicating that the Cu and Co atoms are successfully incorporated into ZnO grains. SEM micrographs show the spherical-like and hexagon-like homogeneous structures. The SEM data are in accordance with the XRD data in terms of average grain size. The samples with higher doping possess poor crystallinity, which may be due to the low ionic radii of Co as compared to those of Zn. This fact also limits further doping. In FTIR spectroscopy, the deviation in the percentage of transmittance of Co−O and Zn−O bands and the characteristic frequency revealed that the addition of *Co* perturbs the structure of the Zn−O−Cu lattice. Strong UV−visible absorption peaks at wavelengths 356, 353, 348, and 319 nm are observed for pure ZnO and $Zn_{0.96-x}Cu_{0.04}Co_xO$ with Co 0%, 2%, and 5%, respectively, and can be generated by the rejoining of excited electrons from localized levels below the conduction band with the holes in the valence band. The band gap is increased from 3.49 to 3.88 eV with increasing doping concentration; this can be interpreted by the Burstein−Moss effect. UV−vis DRS results shows the maximum reflectance for ZnO nanoparticles. In the VSM study, pure ZnO exhibited a diamagnetic behavior, while all the doped samples showed

RTFM. However, the doping of Co decreases the saturation magnetization and retentivity of the sample. This study revealed the fact the ferromagnetic conduct noticed in the Cu and Co co-doped ZnO nanoparticles is an intrinsic property. This research is useful for synthesizing numerous TM-doped ZnO nanoparticles with enhanced optical and magnetic properties for various practical applications of spintronics. Also, further research studies can be carried out to probe both, hole- and electron-mediated ferromagnetism in TM-substituted ZnO, which can be considered to have potential for bipolar spintronics.

EXPERIMENTAL TECHNIQUE AND CHARACTERIZATION

Synthesis Technique. Samples with nominal composition ZnO and $Zn_{0.96-x}Cu_{0.04}Co_xO$ were synthesized using the co-precipitation method, and Co concentration was ranged from 0 to 5%. First, a homogenous mixture was prepared by adding the stoichiometric amounts of $Zn(NO_3)_2 \cdot 6H_2O$ (Sigma-Aldrich), $Cu(NO_3) \cdot 3H_2O$ (Sigma-Aldrich), and $Co(NO_3) \cdot 6H_2O$ (Sigma-Aldrich) in distilled water. All the chemicals were of analytical grade and used as received without extra purification. The solution was constantly stirred for 1 h, and then, required amount of NaOH solution was added to maintain its pH at 9−11. The solution was then mixed under constant stirring for 2 h until white precipitates were formed.

The solution was filtered on filter paper and then washed thoroughly three to five times with deionized water and with ethanol. The resulting solution was again filtered followed by drying at 80 °C for 2 h in an oven. The obtained sample was grounded into a fine powder and annealed at 500 °C for 2 h in a box furnace under air. Four samples ZnO, $Zn_{0.96}Cu_{0.04}O$, $Zn_{0.94}Cu_{0.04}Co_{0.02}O$, and $Zn_{0.91}Cu_{0.04}Co_{0.05}O$ were prepared by following the above procedure.

Characterization Techniques. The structural properties of crystals and phase determination of Co- and Cu-doped ZnO nanoparticles were scanned by using (X'Pert Philips) An X-ray diffractometer by applying Cu Kα radiations (λ = 1.54 Å) at 40 kV and 30 mA from 2θ = 20−80°. The surface morphology of the nanoparticles was attained by using FE-SEM, Quanta FEG

450. FTIR spectroscopy employing Shimadzu IR−Tracer 100 was evaluated in the region 1800−200 cm^{-1} to interpret the infrared spectrum of absorption and reflection. UV−vis spectroscopy was employed to study the optical behavior by using a UV−visible spectrometer (model: lambda 35, Make: PerkinElmer) at room temperature. The evaluation of magnetic properties and vibrational modes (M−H curves) was achieved using a superconducting quantum interference device (SQUID, model MPMS-3 from Quantum Design Inc.) in the State Key Laboratory for Mechanical Behavior of Materials, Xi'an Jiaotong University, China, at room temperature under an applied field of 10 kOe.

■ AUTHOR INFORMATION

Corresponding Authors

Muhammad Tahir Khan − *Department of Physics, Riphah International University, 44000 Islamabad, Pakistan;* Email: zaman.abid87@gmail.com

Abid Zaman − *Department of Physics, Riphah International University, 44000 Islamabad, Pakistan;* ⓞ orcid.org/0000-0001-9527-479X; Email: tahir_iiui14@yahoo.com

Authors

Sidra Kanwal − *Department of Physics, Riphah International University, 44000 Islamabad, Pakistan*

Nasir Mehboob − *Department of Physics, Riphah International University, 44000 Islamabad, Pakistan*

Mongi Amami − *Department of Chemistry College of Sciences, King Khalid University, 61421 Abha, Saudi Arabia; Laboratoire des Matériaux et de l'environnement pour le Développement Durable LR18ES10, 1006 Tunis, Tunisia*

Complete contact information is available at:
https://pubs.acs.org/10.1021/acsomega.2c03375

Notes

The authors declare no competing financial interest.

■ REFERENCES

(1) Pearton, S. J.; Norton, D. P.; Heo, Y. W.; Tien, L. C.; Ivill, M. P.; Li, Y.; Kang, A. F.; Ren, F.; Kelly, J.; Hebard, A. F. ZnO spintronics and nanowire devices. *J. Electron. Mater.* **2006**, *35*, 862−868.

(2) Joshi, V. K. Spintronics: A contemporary review of emerging electronics devices. *Eng. Sci. Technol.* **2016**, *19*, 1503−1513.

(3) Djurišić, A. B.; Ng, A. M. C.; Chen, X. Y. ZnO nanostructures for optoelectronics: Material properties and device applications. *Prog. Quant. Electron.* **2010**, *34*, 191−259.

(4) Zhang, J.; Zhang, L.; Peng, X.; Wang, X. Fabrication of MgO nanobelts using a halide source and their structural characterization. *Appl. Phys. A* **2001**, *73*, 773−775.

(5) Sato, K.; Katayama-Yoshida, H. First principles materials design for semiconductor spintronics. *Semicond. Sci. Technol.* **2002**, *17*, 367.

(6) Panigrahy, B.; Aslam, M.; Bahadur, D. Controlled optical and magnetic properties of ZnO nanorods by Ar ion irradiation. *Appl. Phys. Lett.* **2011**, *98*, 183109.

(7) Bhargava, R.; Sharma, P. K.; Kumar, S.; Pandey, A. C.; Kumar, N. Consequence of doping mediated strain and the activation energy on the structural and optical properties of ZnO: Cr nanoparticles. *J. Solid State Chem.* **2010**, *183*, 1400−1408.

(8) Ghorbani, H. R.; Mehr, F. P.; Pazoki, H.; Rahmani, B. M. Synthesis of ZnO nanoparticles by precipitation method. *Orient. J. Chem.* **2015**, *31*, 1219−1221.

(9) Chand, P.; Gaur, A.; Kumar, A. Effect of Cr and Fe doping on the structural and optical properties of ZnO nanostructures. *Int. J. Chem. Nucl. Mater. Metall. Eng.* **2014**, *8*, 1238−1241.

(10) Jayakumar, O. D.; Gopalakrishnan, I. K.; Kulshreshtha, S. K. The structural and magnetization studies of Co-doped ZnO co-doped with Cu: Synthesized by co-precipitation method. *J. Mater. Chem.* **2005**, *15*, 3514−3518.

(11) Liu, H.; Fei, L.; Liu, H.; Lang, J.; Yang, J.; Liu, Y.; Gao, M.; Liu, X.; Cheng, X.; Wei, M. Effects of annealing atmosphere on structure, optical and magnetic properties of Zn0. 95Cu0. 02Cr0. 03O diluted magnetic semiconductors. *J. Alloys Compd.* **2014**, *587*, 222−226.

(12) Quan, Z.; Li, D.; Sebo, B.; Liu, W.; Guo, S.; Xu, S. Microstructures, surface bonding states and room temperature ferromagnetisms of Zn0. 95Co0. 05O thin films doped with copper. *Appl. Surf. Sci.* **2010**, *256*, 3669−3675.

(13) Hoang, L. H.; Hien, N. T. M.; Hai, N. H.; Hai, P. V.; Khoi, N. T.; Yang, I. S. Raman spectroscopy of Cu doping in Zn1− xCoxO diluted magnetic semiconductor. *J. Raman Spectrosc.* **2009**, *40*, 1535−1538.

(14) Park, M. S.; Min, B. I. Ferromagnetism in ZnO codoped with transition metals: Zn 1− x (FeCo) x O and Zn 1− x (FeCu) x O. *Phys. Rev. B: Condens. Matter Mater. Phys.* **2003**, *68*, 224436.

(15) Huang, L. M.; Rosa, A. L.; Ahuja, R. Ferromagnetism in Cu-doped ZnO from first-principles theory. *Phys. Rev. B: Condens. Matter Mater. Phys.* **2006**, *74*, 075206.

(16) Ashokkumar, M.; Muthukumaran, S. Microstructure and band gap tailoring of Zn0. 96− xCu0. 04CoxO (0≤ x≤ 0.04) nanoparticles prepared by co-precipitation method. *J. Alloys Compd.* **2014**, *587*, 606−612.

(17) Ye, L. H.; Freeman, A. J.; Delley, B. Half-metallic ferromagnetism in Cu-doped ZnO: density functional calculations. *Phys. Rev. B: Condens. Matter Mater. Phys.* **2006**, *73*, 033203.

(18) Ferhat, M.; Zaoui, A.; Ahuja, R. Magnetism and band gap narrowing in Cu-doped ZnO. *Appl. Phys. Lett.* **2009**, *94*, 142502.

(19) Dinesha, M. L.; Jayanna, H. S.; Mohanty, S.; Ravi, S. Structural, electrical and magnetic properties of Co and Fe co-doped ZnO nanoparticles prepared by solution combustion method. *J. Alloys Compd.* **2010**, *490*, 618−623.

(20) Basnet, P.; Samanta, D.; Inakhunbi Chanu, T.; Mukherjee, J.; Chatterjee, S. Assessment of synthesis approaches for tuning the photocatalytic property of ZnO nanoparticles. *SN Appl. Sci.* **2019**, *1*, 633.

(21) Kaur, M.; Kumar, V.; Kaur, P.; Lal, M.; Negi, P.; Sharma, R. Effect on the dielectric properties due to In−N co-doping in ZnO particles. *J. Mater. Sci.: Mater. Electron.* **2021**, *32*, 8991−9004.

(22) Zaman, A.; Uddin, S.; Mehboob, N.; Ali, A. Structural investigation and improvement of microwave dielectric properties in Ca(HfxTi1-x)O3 ceramics. *Phys. Scr.* **2020**, *96*, 025701.

(23) Arshad, M.; Azam, A.; Ahmed, A. S.; Mollah, S.; Naqvi, A. H. Effect of Co substitution on the structural and optical properties of ZnO nanoparticles synthesized by sol−gel route. *J. Alloys Compd.* **2011**, *509*, 8378−8381.

(24) Muthukumaran, S.; Gopalakrishnan, R. Structural, FTIR and photoluminescence studies of Cu doped ZnO nanopowders by co-precipitation method. *Opt. Mater.* **2012**, *34*, 1946−1953.

(25) Liu, H.; Yang, J.; Hua, Z.; Zhang, Y.; Yang, L.; Xiao, L.; Xie, Z. The structure and magnetic properties of Cu-doped ZnO prepared by sol−gel method. *Appl. Surf. Sci.* **2010**, *256*, 4162−4165.

(26) Lupan, O.; Pauporté, T.; Viana, B.; Aschehoug, P. Electro-deposition of Cu-doped ZnO nanowire arrays and heterojunction formation with p-GaN for color tunable light emitting diode applications. *Electrochim. Acta* **2011**, *56*, 10543−10549.

(27) Chakraborti, D.; Narayan, J.; Prater, J. T. Room temperature ferromagnetism in Zn 1− x Cu x O thin films. *Appl. Phys. Lett.* **2007**, *90*, 062504.

(28) Ali, A.; Zaman, A.; Aldulmani, S. A.; Abbas, M.; Mushtaq, M.; Bashir, K.; Amami, K.; Althubeiti, K. Structural Evolution and Microwave Dielectric Properties of Ba1−xSrxTi4O9,(0.0≤ x≤ 0.06) Ceramics. *ACS Omega* **2022**, *7*, 2331−2336.

(29) Kaur, M.; Kumar, V.; Singh, J.; Datt, J.; Sharma, R. Effect of Cu-N co-doping on the dielectric properties of ZnO nanoparticles. *Mater. Technol.* **2022**, 1−15.

(30) Saleem, S.; Jameel, M. H.; Akhtar, N.; Nazir, N.; Ali, A.; Zaman, A. Modification in structural, optical, morphological, and electrical properties of zinc oxide (ZnO) nanoparticles (NPs) by metal (Ni, Co) dopants for electronic device applications. *Arab. J. Chem.* **2022**, *15* (1), 103518.

(31) Essalah, G.; Guermazi, H.; Guermazi, S.; Leroy, G.; Duponchel, B.; Mascot, M.; Mangavati, S. Enhanced dielectric properties of ternary ZnO-based composites for dielectric applications. *Appl. Phys. A* **2022**, *128*, 1−12.

(32) Zaman, A.; Uddin, S.; Mehboob, N.; Tirth, V.; Algahtani, A. Structural Elucidation, Electronic and Microwave Dielectric Properties of Ca(SnxTi1-x)O3, (0 ≤ x ≤ 0.8) Lead-Free Ceramics. *ACS Omega* **2022**, *7*, 4667−4676.

(33) Kaphle, A.; Reed, T.; Apblett, A.; Hari, P. Doping efficiency in cobalt-doped ZnO nanostructured materials. *J. Nanomater.* **2019**, *2019*, 1.

(34) Vijayaprasath, G.; Murugan, R.; Asaithambi, S.; Babu, G. A.; Sakthivel, P.; Mahalingam, T.; Ravi, G. Structural characterization and magnetic properties of Co co-doped Ni/ZnO nanoparticles. *Appl. Phys. A* **2016**, *122*, 122.

(35) Hong, N. H.; Chikoidze, E.; Dumont, Y. Ferromagnetism in laser ablated ZnO and Mn-doped ZnO thin films: A comparative study from magnetization and Hall effect measurements. *Phys. B* **2009**, *404*, 3978−3981.

(36) Vanheusden, K.; Warren, W. L.; Seager, C. H.; Tallant, D. R.; Voigt, J. A.; Gnade, B. E. Mechanisms behind green photoluminescence in ZnO phosphor powders. *J. Appl. Phys.* **1996**, *79*, 7983−7990.

(37) Reddy, A. J.; Kokila, M. K.; Nagabhushana, H.; Chakradhar, R. P. S.; Shivakumara, C.; Rao, J. L.; Nagabhushana, B. M. Structural, optical and EPR studies on ZnO: Cu nanopowders prepared via low temperature solution combustion synthesis. *J. Alloys Compd.* **2011**, *509*, 5349−5355.

(38) Hong, R. Y.; Zhang, S. Z.; Di, G. Q.; Li, H. Z.; Zheng, Y.; Ding, J.; Wei, D. G. Preparation, characterization and application of Fe3O4/ZnO core/shell magnetic nanoparticles. *Mater. Res. Bull.* **2008**, *43*, 2457−2468.

(39) Fu, R.; Wang, W.; Han, R.; Chen, K. Preparation and characterization of γ-Fe2O3/ZnO composite particles. *Mater. Lett.* **2008**, *62*, 4066−4068.

(40) Senol, S. D.; Yalcin, B.; Ozugurlu, E.; Arda, L. Structure, microstructure, optical and photocatalytic properties of Mn-doped ZnO nanoparticles. *Mater. Res. Express* **2020**, *7*, 015079.

(41) van Dijken, A.; Meulenkamp, E. A.; Vanmaekelbergh, D.; Meijerink, A. The kinetics of the radiative and nonradiative processes in nanocrystalline ZnO particles upon photoexcitation. *J. Phys. Chem. B* **2000**, *104*, 1715−1723.

(42) Takagahara, T.; Takeda, K. Theory of the quantum confinement effect on excitons in quantum dots of indirect-gap materials. *Phys. Rev. B: Condens. Matter Mater. Phys.* **1992**, *46*, 15578−15581.

(43) Qin, W.-J.; Sun, J.; Yang, J.; Du, X. W. Control of Cu-doping and optical properties of ZnO quantum dots by laser ablation of composite targets. *Mater. Chem. Phys.* **2011**, *130*, 425−430.

(44) Panigrahy, B.; Aslam, M.; Bahadur, D. Aqueous synthesis of Mn-and Co-doped ZnO nanorods. *J. Phys. Chem. C* **2010**, *114*, 11758−11763.

(45) Potzger, K.; Zhou, S.; Eichhorn, F.; Helm, M.; Skorupa, W.; Mücklich, A.; Fassbender, A.; Herrmannsdörfer, T.; Bianchi, A. Ferromagnetic Gd-implanted ZnO single crystals. *J. Appl. Phys.* **2006**, *99*, 063906.

(46) Sati, P.; Hayn, R.; Kuzian, R.; Régnier, S.; Schäfer, S.; Stepanov, A. Magnetic anisotropy of Co 2+ as signature of intrinsic ferromagnetism in ZnO: Co. *Phys. Rev. Lett.* **2006**, *96*, 017203.

(47) Xia, C. H.; Hu, C. G.; Hu, C. H.; Ping, Z.; Wang, F. Room-temperature ferromagnetic properties of Cu-doped ZnO rod arrays. *Bull. Mater. Sci.* **2011**, *34*, 1083−1087.

(48) Wei, Y.; Hou, D.; Qiao, S.; Zhen, C.; Tang, G. Studies of the physical properties of Co, Cu codoped ZnO powders. *Phys. B* **2009**, *404*, 2486−2488.

(49) Cao, P.; Zhao, D. X.; Shen, D. Z.; Zhang, J. Y.; Zhang, Z. Z.; Bai, Y. Cu+-codoping inducing the room-temperature magnetism and p-type conductivity of ZnCoO diluted magnetic semiconductor. *Appl. Surf. Sci.* **2009**, *255*, 3639−3641.

(50) Spaldin, N. A. Search for ferromagnetism in transition-metal-doped piezoelectric ZnO. *Phys. Rev. B: Condens. Matter Mater. Phys.* **2004**, *69*, 125201.

(51) Sluiter, M. H.; Kawazoe, Y.; Sharma, P.; Inoue, A.; Raju, A. R.; Rout, C.; Waghmare, U. V. First principles based design and experimental evidence for a ZnO-based ferromagnet at room temperature. *Phys. Rev. Lett.* **2005**, *94*, 187204.

(52) Herng, T. S.; Lau, S. P.; Yu, S. F.; Chen, J. S.; Teng, K. S. Zn-interstitial-enhanced ferromagnetism in Cu-doped ZnO films. *J. Magn. Magn. Mater.* **2007**, *315*, 107−110.

(53) Liu, H.; Cheng, X.; Liu, H.; Yang, J.; Liu, Y.; Liu, X.; Gao, Y.; Wei, M.; Zhang, X.; Jiang, Y. Structural, optical and magnetic properties of Cu and V co-doped ZnO nanoparticles. *Phys. E* **2013**, *47*, 1−5.